

PROBING THE RADIAL TEMPERATURE STRUCTURE OF PROTOPLANETARY DISKS WITH HERSCHEL/HIFI*

D. FEDELE¹, S. BRUDERER¹, E.F. VAN DISHOECK^{1,2}, M.R. HOGERHEIJDE², O. PANIC³, J. M. BROWN⁴, TH. HENNING⁵

Draft version August 20, 2018

ABSTRACT

Herschel/HIFI spectroscopic observations of CO $J = 10 - 9$, CO $J = 16 - 15$ and [C II] towards HD 100546 are presented. The objective is to resolve the velocity profile of the lines to address the emitting region of the transitions and directly probe the distribution of warm gas in the disk. The spectra reveal double-peaked CO line profiles centered on the systemic velocity, consistent with a disk origin. The $J = 16 - 15$ line profile is broader than that of the $J = 10 - 9$ line, which in turn is broader than those of lower J transitions ($6 - 5, 3 - 2$, observed with APEX), thus showing a clear temperature gradient of the gas with radius. A power-law flat disk model is used to fit the CO line profiles and the CO rotational ladder simultaneously, yielding a temperature of $T_0 = 1100 \pm 350$ K (at $r_0 = 13$ AU) and an index of $q = 0.85 \pm 0.1$ for the temperature radial gradient. This indicates that the gas has a steeper radial temperature gradient than the dust (mean $q_{dust} \sim 0.5$), providing further proof of the thermal decoupling of gas and dust at the disk heights where the CO lines form. The [C II] line profile shows a strong single-peaked profile red-shifted by 0.5 km s^{-1} compared to the systemic velocity. We conclude that the bulk of the [C II] emission has a non-disk origin (e.g., remnant envelope or diffuse cloud).

Keywords: Protoplanetary disks

1. INTRODUCTION

The temperature distribution of the gas in protoplanetary disks is a fundamental ingredient in models of gas and dust dynamics and the processes which ultimately control disk evaporation and planet formation. Thermo-chemical models of disks show that the gas temperature is significantly higher than that of the dust in the upper layers of the disk, first investigated by Kamp & Dullemond (2004) and Jonkheid et al. (2004) and subsequently by many other groups (e.g., Glassgold et al. 2004; Gorti & Hollenbach 2004; Nomura & Millar 2005; Aikawa & Nomura 2006; Jonkheid et al. 2006, 2007; Gorti & Hollenbach 2008; Ercolano et al. 2009; Woods & Willacy 2009; Voitke et al. 2009; Kamp et al. 2010). These layers also play a key role in the chemical evolution of the disk by forming molecules through high temperature gas-phase reactions (e.g., Aikawa et al. 2002; Voitke et al. 2010). However, the gas temperature in these layers is notoriously difficult to compute and existing models show large differences as reported by Röllig et al. (2007) for the case of PDR models. Disk models span a wider range in gas density and irradiation conditions, with even larger associated uncertainties (see discussion in Visser et al. 2012). Addressing the physical properties

of the gas in these layers directly through observations is thus important to test the various thermo-chemical disk models, which, in turn, provide the basis for the analysis of many other data.

Various observational studies have found evidence for vertical temperature gradients in the gas. The outer disk (> 100 AU) has been probed by single dish (van Zadelhoff et al. 2001) and interferometric data (Dartois et al. 2003; Piétu et al. 2007) of various CO low-lying pure rotational lines. For the inner disk (< 50 AU), evidence for a warm gas layer with $T_{\text{gas}} > T_{\text{dust}}$ was found by Goto et al. (2012) using spectrally and spatially resolved observations of CO ro-vibrational lines. At intermediate radii, the warm layers emit primarily at far-infrared wavelengths. Recent observations with Herschel/PACS report the detections of pure rotational high- J ($J_{\text{u}} > 12$, $E_{\text{u}} \geq 400$ K) CO emission lines in several protoplanetary disks (e.g. Sturm et al. 2010; van Kempen et al. 2010; Meeus et al. 2012, 2013). Modeling of the entire CO ladder for one source, HD 100546, clearly demonstrates the need for gas-dust decoupling in the upper layers throughout most of the disk (Bruderer et al. 2012). However, these spatially unresolved PACS data do not directly probe the radial location of the warm gas. We present here spectrally resolved Herschel/HIFI data that uniquely determine the emitting regions through Kepler's laws.

At a distance of 97 pc (± 4 pc; van Leeuwen 2007), the Herbig Ae star HD 100546 is one of the best studied protoplanetary disks. Bruderer et al. (2012) presented a detailed analysis of the observed CO/CI/CII emission in this source. An unexpected conclusion was that the gaseous carbon abundance in this disk must be ~ 5 times lower than that in the interstellar medium. Their model, however, could not reproduce the strong [C II] emission detected with PACS, even after subtraction of the ex-

* *Herschel* is an ESA space observatory with science instruments provided by European-led Principal Investigator consortia and with important participation from NASA

¹ Max Planck Institut für Extraterrestrische Physik, Giessenbachstrasse 1, 85748 Garching, Germany

² Leiden Observatory, Leiden University, P.O. Box 9513, 2300 RA Leiden, The Netherlands

³ Institute of Astronomy, University of Cambridge, Madingley Road, Cambridge CB3 0HA

⁴ Harvard-Smithsonian Center for Astrophysics, 60 Garden Street, MS 78, Cambridge, MA 02138, USA

⁵ Max Planck Institute for Astronomy, Königstuhl 17, 69117, Heidelberg, Germany

tended [C II] component (Sturm et al. 2010; Fedele et al. 2013). One possibility is that the [C II] flux measured with PACS is contaminated by a compact diffuse component, which can also be tested with spectrally resolved data.

This paper presents new Herschel/HIFI observations of CO $J = 10 - 9$, $J = 16 - 15$ and [C II] toward the Herbig Ae star HD 100546. These spectra are compared to existing APEX sub-millimeter observations of lower- J CO lines ($6 - 5, 3 - 2$, Panić et al. 2010) with the aim of constraining the radial temperature, column density and emitting regions of warm CO and [C II] in the disk and to test the predictions of thermo-chemical models. Given the spread of upper level energy of the four CO lines of more than one order of magnitude, with $E_{J=3} = 33$ K and $E_{J=16} = 751$ K, a large range of temperatures can be probed.

2. OBSERVATIONS AND DATA REDUCTION

The CO $J = 16 - 15$ (obsid: 1342247519), CO $J = 10 - 9$ (1342235779) and [C II] (1342247518) observations were executed in dual beam switch fast chopping mode with the Wide-Band Spectrometer (WBS) and the Heterodyne Instrument for the Far-Infrared (HIFI) simultaneously. The spectral resolution was set to 1.1 MHz for WBS and 0.25 MHz for HRS for both polarizations. Because of the diffuse [C II] emission, seen previously with PACS, the [C II] observation of has been carried out in “load chop” where an internal calibration source is used in combination with an “off-source” calibration observation. The half-power-beam-width (HPBW) is $18''.9$ at the frequency of the CO $J = 10 - 9$ line and $11''.1$ at the frequencies of the CO $J = 16 - 15$ and [C II] lines (Roelfsema et al. 2012), thus the beam encompasses the entire disk.

The spectra have been extracted from the level 2 data which have been processed with standard pipeline SPG v9.1.0. Standing waves are present in the WBS and HRS band 7 spectra of the CO $J = 16 - 15$ and [C II] lines. These have been removed by fitting a set of sine functions after masking the narrow spectral features (CO or [C II]). This operation was performed with the ‘fitHifiFringe’ script provided with Hipe. No significant differences are observed in the two polarizations and the final spectra are obtained by averaging the two polarizations (for WBS and HRS separately). The data are converted from antenna temperature to mean-beam temperature (T_{mb}) dividing by η_A/η_l , where η_A is the beam efficiency (0.56 for CO $J = 10 - 9$ and 0.62 for CO $J = 16 - 15$ and [C II], respectively) and η_l is the forward efficiency, 0.96 (Roelfsema et al. 2012). The spectra are shown in Fig. 1.

3. RESULTS

The CO $J = 16 - 15$, CO $J = 10 - 9$ and [C II] lines are detected in the WBS spectrum. The [C II] line is also detected in the HRS spectrum.

3.1. CO

The HIFI/WBS spectra of the CO lines are shown in Fig. 1 (top 2 panels), normalized to their peak intensity. The profiles of both lines show a characteristic double-peak profile created by the Keplerian motion of the gas in the protoplanetary disk around HD 100546. The lines are

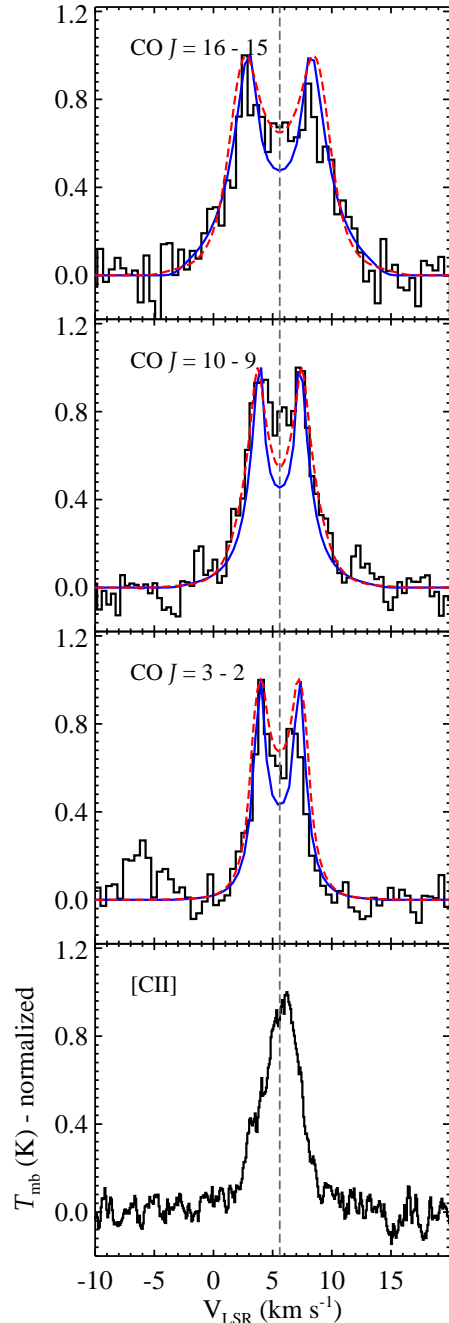


Figure 1. Herschel/HIFI spectra of CO $J = 16 - 15$, $J = 10 - 9$ and [C II] toward HD 100546, together with the APEX $J = 3 - 2$ spectrum (from Panić et al. 2010). The vertical dashed line shows the system velocity. The (blue) solid line is the best fit power-law model (§ 4) and the (red) dashed is the prediction of the thermo-chemical model from Bruderer et al. (2012).

centered at $V_{\text{LSR}} = 5.6 \text{ km s}^{-1}$ in good agreement with the system velocity measured using low- J CO lines in the sub-millimeter (e.g. Panić et al. 2010). The $J = 16 - 15$ line is clearly broader than the $J = 10 - 9$ line. The integrated intensities and fluxes⁷ are reported in Table 1.

⁷ To convert the integrated intensity ($\int T_{mb} dV$, K m s^{-1}) to integrated flux (W m^{-2}), the conversion formula is $2 k \left(\frac{\nu}{c}\right)^3 \pi \left(\frac{HPBW}{2\sqrt{\ln(2)}}\right)^2 \int T_{mb} dV$, with k (Boltzmann constant) in unit of W s K^{-1} , ν in Hz , c in m s^{-1} , T_{mb} in K .

Table 1

Parameters of the CO line emission. $R_{25\%}$ and $R_{75\%}$ indicate the radii encircling 25% and 75% of the emission as measured from the cumulative distribution (Fig. 3).

Transition	ν [GHz]	E_u [K]	HPBW [$''$]	Δv_{peak}^a [km s^{-1}]	FWHM [km s^{-1}]	Int. Intensity [K km s^{-1}]	Integrated Flux [$10^{-17} \text{ W m}^{-2}$]		$R_{25\%}$ [AU]	$R_{75\%}$ [AU]	
							PL ^c	TC ^d			
CO $J=16-15$	1841.345	751	11.1	5.3	8.2	2.8 ± 0.08	5.9 ± 0.2	7.68	8.72	30	90
CO $J=10-9$	1151.985	304	18.9	3.4	5.7	3.0 ± 0.09	4.5 ± 0.2	5.11	5.68	70	230
CO $J=6-5$	691.472	114	9.1	2.4	4.2	17.7 ± 0.9^b	1.32 ± 0.07^b	1.35	1.76	115	300
CO $J=3-2$	345.796	33	18.2	2.4	4.0	4.0 ± 0.6^b	0.15 ± 0.02^b	0.14	0.26	150	320
[C II]	1900.537	91	11.1		3.7	8.5 ± 0.15	19.6 ± 0.4				

^a Peak-to-peak velocity separation

^b Panić et al. (2010)

^c Line flux predicted by the best-fit power-law model (§ 4).

^d Line flux predicted by the thermo-chemical model by Bruderer et al. (2012) (§ 5).

The flux of the CO $J = 16 - 15$ line agrees well with the Herschel/PACS measurement ($5.88 \pm 0.97 \cdot 10^{-17} \text{ W m}^{-2}$, Meeus et al. 2013). The third panel of Fig. 1 shows the $J = 3 - 2$ sub-millimeter line, which is narrower than both higher- J lines with a velocity width of only $\Delta v_{\text{peak}} = 2.4 \text{ km s}^{-1}$ (Δv_{peak} refers to the peak-to-peak separation). Table 1 summarizes the observed widths with the maximum velocity broadening observed in the $J = 16 - 15$ line ($\Delta v = 5.3 \text{ km s}^{-1}$). Because of high disk inclination (42°), the Keplerian motion dominates the line width, meaning that the narrow lowest- J line traces the slowly rotating gas in the outer part of the disk and the wider highest- J line traces faster gas located closer to the star.

3.2. [C II]

The [C II] spectrum is shown in Fig. 1 with a spectral resolution of 1.1 MHz (0.17 km s^{-1}). At this resolution the line does not reveal a double peaked profile characteristic of Keplerian motion. Moreover, because the line is centered $\sim 0.5 \text{ km s}^{-1}$ redward of the known system velocity, it is very likely that most of the [C II] line does not come from the disk.

4. ANALYSIS

The simplest possible model to analyze both the velocity profiles as well as the line intensities is a geometrically thin disk model in which temperature and column density are power-law functions of radius. The CO velocity profiles then constrain the radial temperature gradient of the gas while the line fluxes provide further constraints to the radial distribution of the gas column density. Specifically,

$$N(r) = N_0 \left(\frac{r}{r_0} \right)^{-p} \quad T(r) = T_0 \left(\frac{r}{r_0} \right)^{-q} \quad (1)$$

where r_0 is the inner radius of the disk, 13 AU as found by van der Plas et al. (2009), and N_0 , T_0 are the column density and temperature at r_0 . The motivation to use a geometrically thin disk is the fact that full thermochemical models (e.g. Bruderer et al. 2012) show that the high- J pure rotational CO lines emerge from a narrow range in heights. The free parameters of the model are N_0 , T_0 , p , q . The model assumptions are: 1) the gas is in Keplerian rotation; 2) CO excitation is thermalized (because of the low values of the line critical density,

this assumption holds for all the CO lines analysed here, Bruderer et al. 2012; 3) the intrinsic line shape is Gaussian and the intrinsic width at each position is given by the thermal broadening plus turbulent broadening (fixed to $v_{\text{turb}} = 0.3 \text{ km s}^{-1}$).

4.1. Line flux from a rotating disk

The line flux from a rotating disk is given by the integral over the disk surface

$$F_\nu = \frac{\cos(i)}{d^2} \int_{r_{\text{in}}}^{r_{\text{out}}} \int_0^{2\pi} B_\nu(T(r)) \left(1 - e^{-\tilde{\tau}(r,\theta)} \right) d\theta r dr \quad (2)$$

which is defined by polar coordinates (r and θ). The line opacity is

$$\tilde{\tau}(r, \theta) = \frac{\tau(r)_{\nu-\nu/c \cdot v_{\text{proj}}(r,\theta,i)}}{\cos(i)} \quad (3)$$

with i (42°) the disk inclination ($i = 0^\circ$ is edge on), d the distance, $B_\nu(T(r))$ the Planck function and $\tau(r)$ the opacity perpendicular to the disk surface. For a Keplerian rotating disk around a star with mass M_* ($2.5 M_\odot$), the projected velocity is

$$v_{\text{proj}}(r, \theta, i) = \sqrt{\frac{GM_*}{r}} \sin(i) \cos(\theta) \quad (4)$$

The opacity of a line connecting two CO levels u and l is given by

$$\tau_\nu = \frac{A_{ul} c^2}{8\pi\nu^2} N(r) \left(x_l \frac{g_u}{g_l} - x_u \right) \times \frac{1}{\sqrt{\pi} \Delta\nu} e^{-\left(\frac{\nu}{\Delta\nu}\right)^2} \quad (5)$$

where A_{ul} is the Einstein-A coefficient, $x_{l,u}$ the normalized level population, $g_{u,l}$ the statistical weights and $\Delta\nu$ the intrinsic line width (Doppler-parameter). The molecular data are from Schöier et al. (2005). Assuming local thermodynamic equilibrium, the level population is given by $x_i = g_i \exp(-E_i/kT)/Q(T)$, with the level energy E_i and the partition function $Q(T)$. The telescope beam is represented by a Gaussian. The intrinsic line width contains contributions from turbulent and thermal broadening. The model profiles of the three lines are shown in Fig. 1.

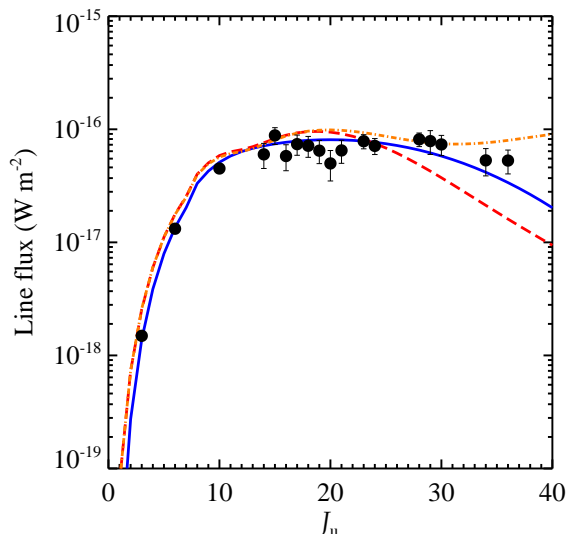


Figure 2. The observed CO rotational ladder (Sturm et al. 2010; Meeus et al. 2013) together with model fits. The (blue) solid line shows the best-fit power-law model, the (red) dashed line shows the prediction of the *standard* thermo-chemical model from Bruderer et al. (2012) while the (orange) dot-dashed line shows the same model with a different H_2 formation rate (§ 5).

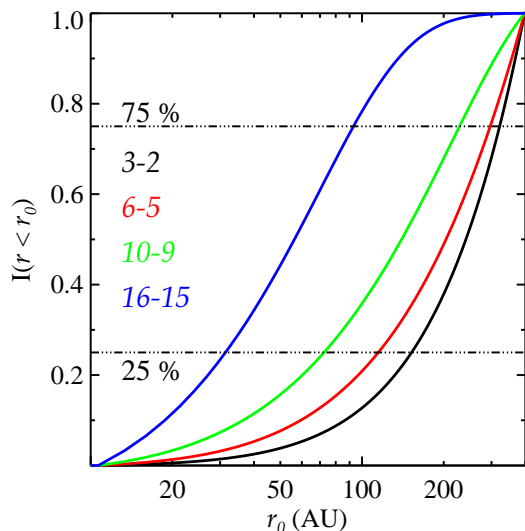


Figure 3. Cumulative distribution of the 4 CO lines as predicted by the power-law model. The dot-dashed lines indicate the 25% and 75% limits.

4.2. CO velocity profiles and rotational ladder

The fit of the CO ladder by itself is degenerate as different power-law indices are able to reproduce the line fluxes. The resolved profiles of the CO lines are needed to break this degeneracy. The best-fit parameters are found by minimizing the χ^2 (sum of the 5 individual χ^2 , 4 for the velocity profiles and 1 for the line fluxes from the CO rotational ladder). The χ^2 minimization is performed in 2 steps: first a sparse grid of 10000 models was created for 10 different values of the parameters in the following ranges: T_0 between 500–1400 K (step of 100 K), N_0 between $10^{16} - 10^{20} \text{ cm}^{-2}$, p, q between 0.5 – 1.4 (step of 0.1). The minimum χ^2 defines the initial guess of the best-fit parameters. In a second step, a denser

grid of models (again 10000) is created around the initial guesses. The best-fit parameters are: $T_0 = 1100 \pm 350 \text{ K}$, $q = 0.85 \pm 0.1$, $N_0 = 5 \pm 3 \times 10^{17} \text{ cm}^{-2}$, $p = 0.9 \pm 0.3$. The parameter uncertainties correspond to the 1σ confidence level⁸. The temperature radial gradient is well constrained thanks to the resolved velocity profiles (values of $q < 0.6$ are excluded at 3σ level). The column density is poorly constrained because the low- J lines (up to $J = 16 - 15$) are optically thick (Bruderer et al. 2012).

The best-fit model is plotted in Figs. 1 and 2 (blue solid line); the same power-law model reproduces the line velocity profiles and the overall shape of the rotational ladder. This simple model, however, produces too strong central absorption at low velocities (see discussion in § 5).

Fig. 3 (left) shows the cumulative distribution of the different CO transitions. The dot-dashed lines show the 25% and 75% limits and the corresponding radii are given in Table 1. The values of $R_{25\%}$ and $R_{75\%}$ indicate the radial distances in the disk where most of the line emission comes from: the $J = 3 - 2$ line emerges mainly from the outer disk (150 – 320 AU) while the highest- J line presented here emerges at intermediate radii (30 – 90 AU).

5. COMPARISON TO THERMO-CHEMICAL MODELS

The knowledge of the temperature and column density radial distribution of warm gas is important for our understanding of the disk internal structure. How do these observational results compare with gas temperatures of thermo-chemical models? The (red) dashed lines in Figs. 1 and 2 show the prediction of the *standard* thermo-chemical model of Bruderer et al. (2012) for the HD 100546 disk (corresponding to the representative model, discussed in § 3 of that paper). The model results agree well with the observed line profiles. Specifically, it reproduces quantitatively the increasing width of the lines with increasing J . It also provides a better fit to the profiles than the power-law model at low-velocities because it accounts for the vertical structure of the disk. A related result of the full disk model is the decreasing emitting area of the lines with increasing J as a consequence of the thermal gradient in the radial direction: Bruderer et al. (2012) estimated that the 75% of the $J = 16 - 15$ line emerges from a ring between 35 – 80 AU while the $J = 3 - 2$ line emerges from a ring between 70 – 220 AU, close to the inferred values.

The thermo-chemical model reproduces the overall shape of rotational ladder up to the mid- J lines ($J = 24 - 23$), but it underestimates the flux of higher- J lines. As discussed in Bruderer et al. (2012, § 4, 5) the flux of higher- J lines depends on the adopted H_2 formation rate. In Fig. 2 we also show the fluxes of a model with a parametrized H_2 formation prescribed following Jonkheid et al. (2004) with $T_{\text{form}} = 1600 \text{ K}$ (orange dot-dashed line). This model reproduces also the higher- J lines and it agrees well with the observed velocity profiles.

The value of q derived here indicates a steeper radial gradient of the gas temperature compared to the

⁸ The 1σ confidence level is given by the $\Delta\chi^2 = 1$ region, which corresponds to the confidence interval of each of the four parameters taken separately from the others (e.g., Bevington & Robinson 2003).

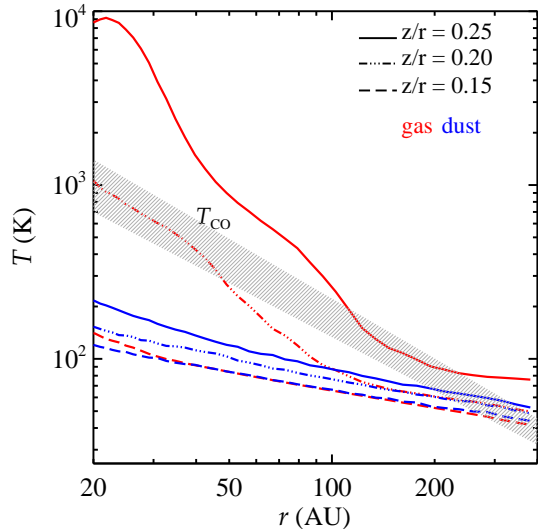


Figure 4. Model predictions of the temperature radial gradient of gas (red) and dust (blue) at 3 different heights in the disk of HD 100546 (from Bruderer et al. 2012). The dashed area shows the range of best-fit power-law models.

dust power-law index derived by interferometric observations at millimeter wavelengths (mean $q_{\text{dust}} \sim 0.5$, e.g. Andrews & Williams 2007; Hughes et al. 2008; Isella et al. 2009). The different radial gradient is likely due to the fact that the observed CO lines emerge from higher up in the disk compared to the mm dust emission which traces the disk mid-plane (where $T_{\text{gas}} = T_{\text{dust}}$). In these layers, the thermo-chemical models suggest high inner temperature (T_0 , because of, e.g., photoelectric heating) and steep radial gradient (q) because of the thermal-decoupling of gas and dust. This is shown in Fig. 4 where the gas and dust temperature radial gradients are plotted for 3 different heights (z/r) in the disk relevant to the CO line formation. The power-law model overlaps with the thermo-chemical model at $z/r = 0.2$ in the inner region ($r < 50$ AU) and at $z/r = 0.25$ in the outer disk ($r > 100$ AU). Overall, our empirical gas temperature distribution provides a benchmark for future thermo-chemical models.

Another important test for the thermo-chemical models is the nature of the [C II] emission on HD 100546. Based on the non-detection of [C I], Bruderer et al. (2012) speculated that the disk lacks volatile carbon (i.e., carbon not locked up in refractory carbonaceous grains) compared to the ISM. One option is that CO ice has been transformed to CH_3OH and more complex ice species during the cold collapse phase of the cloud. Their model predicts the [C II] emission associated with the disk to be almost an order of magnitude fainter than observed with PACS (after subtraction of the spatially extended emission). Our finding that most of the [C II] flux measured with PACS and HIFI has a non-disk origin (Fig. 1, sec. 3.2) is consistent with this hypothesis.

6. CONCLUSIONS

In this letter, we have used spectrally resolved observations of different CO lines to constrain the radial temperature gradient of the warm gas in the disk around HD 100546. *Facilities:* Herschel

100546. The spectrally resolved CO lines show a velocity broadening consistent with the predictions of full thermo-chemical disk models (Bruderer et al. 2012). These observations therefore provide a new probe of the thermal decoupling of gas and dust as revealed by the high inner CO temperature (T_0) and steep temperature gradient (q). The HIFI [C II] spectrum confirms that the line flux measured with PACS is significantly contaminated by compact diffuse material.

REFERENCES

- Aikawa, Y., & Nomura, H. 2006, *ApJ*, 642, 1152
Aikawa, Y., van Zadelhoff, G. J., van Dishoeck, E. F., & Herbst, E. 2002, *A&A*, 386, 622
Andrews, S. M., & Williams, J. P. 2007, *ApJ*, 659, 705
Bevington, P. R., & Robinson, D. K. 2003, *Data reduction and error analysis for the physical sciences*
Bruderer, S., van Dishoeck, E. F., Doty, S. D., & Herczeg, G. J. 2012, *A&A*, 541, A91
Dartois, E., Dutrey, A., & Guilloteau, S. 2003, *A&A*, 399, 773
Ercolano, B., Clarke, C. J., & Drake, J. J. 2009, *ApJ*, 699, 1639
Fedele, D., et al. 2013, *ArXiv e-prints*
Glassgold, A. E., Najita, J., & Igea, J. 2004, *ApJ*, 615, 972
Gorti, U., & Hollenbach, D. 2004, *ApJ*, 613, 424
—. 2008, *ApJ*, 683, 287
Goto, M., et al. 2012, *A&A*, 539, A81
Hughes, A. M., Wilner, D. J., Qi, C., & Hogerheijde, M. R. 2008, *ApJ*, 678, 1119
Isella, A., Carpenter, J. M., & Sargent, A. I. 2009, *ApJ*, 701, 260
Jonkheid, B., Dullemond, C. P., Hogerheijde, M. R., & van Dishoeck, E. F. 2007, *A&A*, 463, 203
Jonkheid, B., Faas, F. G. A., van Zadelhoff, G.-J., & van Dishoeck, E. F. 2004, *A&A*, 428, 511
Jonkheid, B., Kamp, I., Augereau, J.-C., & van Dishoeck, E. F. 2006, *A&A*, 453, 163
Kamp, I., & Dullemond, C. P. 2004, *ApJ*, 615, 991
Kamp, I., Tilling, I., Woitke, P., Thi, W.-F., & Hogerheijde, M. 2010, *A&A*, 510, A18
Meeus, G., et al. 2012, *A&A*, 544, A78
—. 2013, *ArXiv e-prints*
Nomura, H., & Millar, T. J. 2005, *A&A*, 438, 923
Panić, O., van Dishoeck, E. F., Hogerheijde, M. R., Belloche, A., Güsten, R., Boland, W., & Baryshev, A. 2010, *A&A*, 519, A110
Piétu, V., Dutrey, A., & Guilloteau, S. 2007, *A&A*, 467, 163
Roelfsema, P. R., et al. 2012, *A&A*, 537, A17
Röllig, M., et al. 2007, *A&A*, 467, 187
Schöier, F. L., van der Tak, F. F. S., van Dishoeck, E. F., & Black, J. H. 2005, *A&A*, 432, 369
Sturm, B., et al. 2010, *A&A*, 518, L129
van der Plas, G., van den Ancker, M. E., Acke, B., Carmona, A., Dominik, C., Fedele, D., & Waters, L. B. F. M. 2009, *A&A*, 500, 1137
van Kempen, T. A., et al. 2010, *A&A*, 518, L121
van Leeuwen, F. 2007, *A&A*, 474, 653
van Zadelhoff, G., van Dishoeck, E. F., Thi, W., & Blake, G. A. 2001, *A&A*, 377, 566
Visser, R., et al. 2012, *A&A*, 537, A55
Woitke, P., Kamp, I., & Thi, W. 2009, *A&A*, 501, 383
Woitke, P., Pinte, C., Tilling, I., Ménard, F., Kamp, I., Thi, W.-F., Duchêne, G., & Augereau, J.-C. 2010, *MNRAS*, 405, L26
Woods, P. M., & Willacy, K. 2009, *ApJ*, 693, 1360